CrystEngComm

Cite this: *CrystEngComm*, 2012, **14**, 4507–4512

www.rsc.org/crystengcomm

PAPER

Photocatalytic studies of CdS nanoparticles assembled on carbon microsphere surfaces with different interface structures: from amorphous to graphite-like carbon†

Yu Liu,‡[a] Mojiao Zhou,‡[a] Yong Hu,*[a] Haisheng Qian,[a] Jiafu Chen[b] and Xiao Hu*[c]

Received 14th March 2012, Accepted 5th April 2012
DOI: 10.1039/c2ce25369k

A rapid microwave-assisted method was used for the accurate coating of CdS nanoparticles on the surface of colloidal carbon microspheres to form C/CdS hybrid microspheres, which demonstrated enhanced visible-light-photocatalytic activity for the degradation of rhodamine B (RhB). To investigate the optimal photocatalytic synergistic effect, the above as-prepared of C/CdS hybrid microspheres were treated in a tube furnace by annealing at different temperatures (from 300 to 800 °C) in a N_2 flow, which resulted in CdS nanoparticles assembled on different carbon layers (from amorphous to graphite-like carbon). The changes in FT-IR and Raman spectra that were caused by different interfaces were studied. Further, the synergic effect between CdS nanoparticles and different carbon layers, which influence the photocatalytic activity, was then investigated systematically. The results show that the photocatalytic activity of these samples was gradually enhanced as the calcination temperature increased. But compared to the sample without calcination, the photocatalytic activity decreases first and then increases. The combination of CdS and graphite-like carbon may be an ideal system to cause a rapid photoinduced charge separation and decreased possibility of recombination of electron–hole pairs by taking advantage of graphite-like carbon's unique electron transport properties, which increase the number of holes participating in the photooxidation process and enhance the photocatalytic activity.

Introduction

During the past decades, the photocatalytic degradation of organic compounds has been extensively studied for its potential for environmental remediation. Meanwhile, a great deal of metal oxide and sulfide semiconductors are found to be used as photocatalysts in purifying wastewater.[1–3] As a II–VI semiconductor compound, cadmium sulfide (CdS) has attracted considerable interest in optoelectronic applications because of its band gap energy (2.42 eV) in the visible-light region.[4,5] CdS is also generally considered to be one of the best photocatalysts for its unique photochemical and photophysical properties such as high-efficiency, photochemical stability, and low-cost in wastewater treatment.[6,7] Unfortunately, the photocatalytic activity of pure CdS is limited due to its poor adsorption abilities and the fast recombination rates of photoinduced charge carriers. For improving the photocatalytic activity of CdS, the processes in the photocatalytic reaction, including the generation, separation, recombination and migration of the photogenerated electrons and holes, should be comprehensively investigated.[8,9] Several methods have been employed for improving the photocatalytic activity of CdS such as metal cation doping, surface modification with metals, and addition of semiconducting metal oxides.[10–12] However, enhancing the photocatalytic efficiency of CdS to meet the practical application requirements is still a challenge because of the need for the enhancement of solar energy conversion and the suppression of the recombination of photogenerated electron–hole pairs.

It is widely accepted that a high mobility for photoexcited electron–hole separation is very important and has significant benefits for the improvement of the catalytic performance of photocatalysts.[13,14] Conjugated materials have been proven to be a category of materials with unique properties in electron or hole transport, which can cause a rapid photoinduced charge separation and a relatively slow charge recombination in electron-transfer processes.[15–17] Graphite-like carbon has a conjugated structure and the combination of semiconductors and graphite-like carbon may be an ideal system to accelerate the charge transfer from photocatalyst to the liquid–solid interface contacting with organic pollutants by taking advantage of carbon's unique electron transport properties. Several recent publications have reported that graphite-like carbon loading on

[a]*Institute of Physical Chemistry, Zhejiang Normal University, Jinhua, 321004, P. R. China. E-mail: yonghu@zjnu.edu.cn*
[b]*Hefei National Laboratory for Physical Sciences at Microscale, University of Science and Technology of China, Anhui, 230026, P. R. China*
[c]*School of Materials Science & Engineering, Nanyang Technological University, Singapore, 639798, Singapore. E-mail: asxhu@ntu.edu.sg*
† Electronic supplementary information (ESI) available. See DOI: 10.1039/c2ce25369k
‡ These authors contributed equally to this work.

photocatalysts could be used as an electron transfer channel for reducing the recombination of the photogenerated electron–holes, and leading to improved photoconversion efficiency of the photocatalytic materials. Zhu's group have developed conjugative π structure materials hybridized with semiconductor as efficient photocatalysts, they coated TiO_2 and ZnO particles *via* hybridization with graphite-like carbon, which obviously enhanced the photocatalytic activity of pure TiO_2 and ZnO.[18,19] Li *et al.* reported that carbon-modified Bi_2WO_6 showed excellent photoactivity activity towards rhodamine B (RhB) by enhancing the photogenerated electron–hole separation associated with the carbon layer.[20] Although preparation of graphitic-like carbon modified semiconductors and enhanced photocatalytic activity have been reported, little attention was paid to the synergic effect between graphitic-like carbon and CdS.

Recently, we reported a rapid microwave-assisted method for the accurate coating of CdS nanoparticles on the surface of colloidal carbon microspheres to form C/CdS hybrid spheres,[21] which demonstrate enhanced visible-light-photocatalytic activity for the degradation of RhB. However, the photocatalytic mechanism caused by the interface of the CdS nanoparticles and carbon layer needs further investigation. In this paper, based on the previous research, we treated the as-prepared C/CdS hybrid microspheres in a tube furnace by annealing at different temperatures in a N_2 atmosphere, and we removed samples with different calcination temperatures of 300, 400, 500, 600, 700, and 800 °C for testing. The changes in FT-IR and Raman spectra that were caused by different interfaces were studied. Moreover, the synergic effect between CdS nanoparticles and different carbon layers and the resulting impact on the photocatalytic activity were then investigated systematically.

Materials and methods

All reagents in this work were analytical grade, purchased from the Shanghai Chemical Reagent Factory, and used as received without further purification.

Synthesis of C/CdS core–shell hybrid microspheres *via* microwave irradiation and graphitization treatment

The C/CdS core–shell hybrid microspheres were synthesized in a similar way to that which we presented previously.[21] Briefly, 0.01 mol of $CdCl_2{\cdot}2.5H_2O$ was added into a round-bottom flask and dissolved in a solvent containing 10 mL of ethanol and 10 mL of distilled water, which formed a clear solution. A 25 mg portion of the as-prepared carbon microspheres obtained by the reported method[22] was added into the above solution and well dispersed with the assistance of ultrasonication for 10 min. The Cd-absorbed carbon microspheres solution was maintained at 60 °C for 12 h to arrive at the saturated extent of adsorption and then was collected by centrifugation. To remove possible superfluous cations and anions, the obtained products were washed with ethanol and distilled water three times, and then dried at 80 °C for 4 h. 20 mL of the above-mentioned ion-absorbed template suspension, and 0.01 mol of thioacetamide (TAA) were placed in a microwave refluxing system and irradiated at 280 W for 30 min. The C/CdS core–shell hybrid microspheres were thereby obtained. After collection by centrifugation, the final products were washed with ethanol and distilled water three times before drying at 80 °C for 4 h.

Then, the graphitization process was achieved in a tube furnace by annealing the above samples at different temperatures (300, 400, 500, 600, 700, and 800 °C) for 3 h in a N_2 flow (60 mL min^{-1}). The products obtained at temperatures of 300, 400, 500, 600, 700, and 800 °C were named as S-300, S-400, S-500, S-600, S-700, and S-800, respectively, and the original sample without calcination was named S-0.

Characterization

Powder X-ray diffraction (XRD) measurements of the samples were performed with a Philips PW3040/60 X-ray diffractometer using Cu-Kα radiation at a scanning rate of 0.06 deg s^{-1}. Scanning electron microscopy (SEM) was performed with a Hitachi S-4800 scanning electron micro-analyzer with an accelerating voltage of 15 kV. Transmission electron microscopy (TEM) was conducted at 200 kV with a JEM-2100F field emission TEM. Fourier transform infrared (FT-IR) spectroscopy was carried out using Nicolet NEXUS670 spectrometer in the frequency range of 4000–400 cm^{-1}. The photoluminescence (PL) spectra were recorded on an Edinburgh FLSP920 fluorescence spectrometer, and the absorption spectra were measured using a PerkinElmer Lambda 900 UV-vis spectrophotometer at room temperature. Raman spectra were collected by a Renishaw RM1000 confocal microprobe under ambient conditions, and the excitation wavelength was 514 nm.

Photochemical experiments

The photocatalytic activities of the as-prepared samples were evaluated by the degradation of RhB under visible light irradiation of a 500 W Xe lamp with a 420 nm cutoff filter. The reaction cell was placed in a sealed black box with the top opened, and the cutoff filter was placed to provide visible-light irradiation. In a typical process, 0.04 g of as-prepared samples as photocatalysts were added into 100 mL of RhB solution (concentration: 5 mg L^{-1}). After being dispersed in an ultrasonic bath for 5 min, the solution was stirred for 2 h in the dark to reach adsorption equilibrium between the catalyst and the solution and then was exposed to visible light irradiation. The samples were collected by centrifugation at given time intervals to measure the RhB degradation concentration by UV-vis spectroscopy.

Results and discussion

The XRD patterns of a series of C/CdS hybrid microspheres obtained microwave-assisted method, and then calcination at different temperatures, are shown in Fig. 1. The peaks at 2θ values of 26.4, 43.9, and 51.9° correspond to the (111), (220), and (311) crystal planes, respectively, of face-centered cubic (fcc) CdS (JCPDS standard card no. 89-0440) with a cell constant of a = 5.811 Å. In addition, the broad peak at around 26° (d = 0.34 nm) also indicates the characteristic (002) peak of 2D graphitic structures,[23] that occurs in the same place as the sharp (111) peak of CdS. Thus, we calculate the CdS particle size from the second CdS peak. The average size of CdS nanoparticles is gradually increased as the calcination temperature is increased, which is

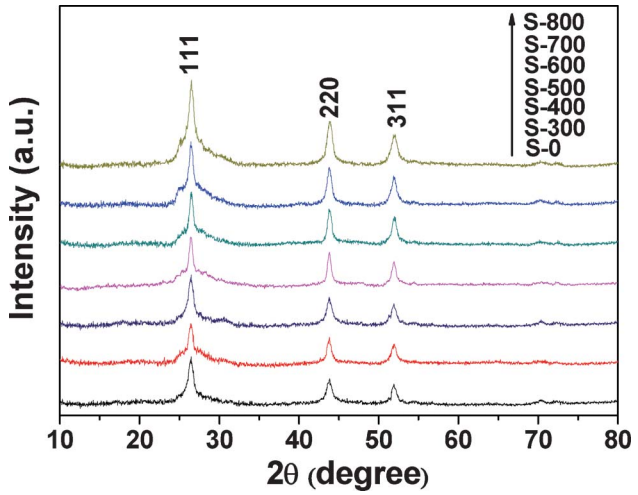

Fig. 1 XRD patterns of as-prepared C/CdS hybrid microspheres and samples after calcination at different temperatures in a N_2 flow.

calculated using the Debye–Scherrer equation based on the full width at half-maximum of the diffraction peak and displayed in Table 1. It is well known that cubic CdS is a metastable phase, which could easily transform from cubic phase to hexagonal phase at a higher temperature. The XRD patterns of the as-prepared pure CdS obtained *via* the microwave-assisted method[21] before and after calcination at 300 °C are shown in Fig. S1 (See ESI†). It can be seen that the pure CdS without carbon core easily transforms from cubic to hexagonal phase after annealing at 300 °C in a N_2 flow. However, the cubic phase of CdS is sustained in these hybrid structures even at a higher temperature in a N_2 flow in our experiment, which indicates that carbon may be helpful to improve its stability. Similar phenomena have been reported by Shanmugam *et al.*, which demonstrate that carbon could effectively suppress the phase transformation of TiO_2 under high temperatures.[24]

The SEM images of carbon microspheres, the C/CdS hybrid spheres synthesized *via* a microwave-assisted method and after calcination at different temperatures in a N_2 flow for 3 h are shown in Fig. 2. Fig. 2a shows the pure carbon spheres of about 1 μm in diameter with smooth surfaces. From Fig. 2b–f, obvious morphological changes can be observed. With increasing calcination temperature, the surface of the colloidal carbon spheres became rougher and more cementitious, which demonstrates that the CdS nanoparticles grow gradually and this result is consistent with that of XRD. Fig. 3a shows typical TEM images of nearly monodisperse C/CdS hybrid microspheres obtained *via* a rapid microwave-assisted route. From the higher magnification image (inset in Fig. 3a), it is obvious that monodisperse CdS nanoparticles are well distributed on the surface of the carbon microspheres. The TEM images of as-prepared samples after calcination at different temperatures in a N_2 flow for 3 h (Fig. 3b–f) show that a large amount of CdS nanoparticles aggregate together and become more cementitious as the calcination temperature is increased, and the HRTEM image (inset in Fig. 3f) also displays the CdS nanoparticles congregated together. Thus, the large increase of the 'grainy' roughness from the SEM image is not due to an increase in the

Table 1 The degree of graphitization of the as-prepared C/CdS hybrid microspheres and CdS nanoparticles size after calcination at different temperatures

Sample	Degree of graphitization $I_{D\text{-band}}/I_{G\text{-band}}$ [a.u.]	CdS nanoparticle size/nm[a]
S-0	0.815	9.70
S-300	0.867	10.1
S-400	0.880	10.6
S-500	0.889	11.8
S-600	0.926	12.7
S-700	0.976	13.3
S-800	0.979	14.9

[a] CdS particle size was calculated from XRD diffraction data.

CdS crystal size alone. It is due to the cementitious aggregate of CdS nanoparticles under high temperatures.

The nature of the changes of the interface in the samples was also investigated by Raman spectroscopy, as shown in Fig. 4. All the spectra show two peaks around 1339 and 1590 cm^{-1}. The G-bands at around 1590 cm^{-1} could be attributed to the characteristic ordered graphitic-like carbon, and the D-band at around 1344 cm^{-1} could be attributed to the presence of defects within the hexagonal graphitic structure. Compared with the spectra of pure graphite crystals (1575 cm^{-1}), the G-band shifted to higher wave numbers in all sample spectra, which suggests some structural imperfections of the carbon cores.[18,19] The intensity ratio of D- and G-band ($I_{D\text{-band}}/I_{G\text{-band}}$) is indicative of the degree of graphitization and its value for each sample is displayed in Table 1. Since the intensities of the G-bands are comparable to those of the D-bands, we conclude that the samples have some degree of atomic-scale ordering. This

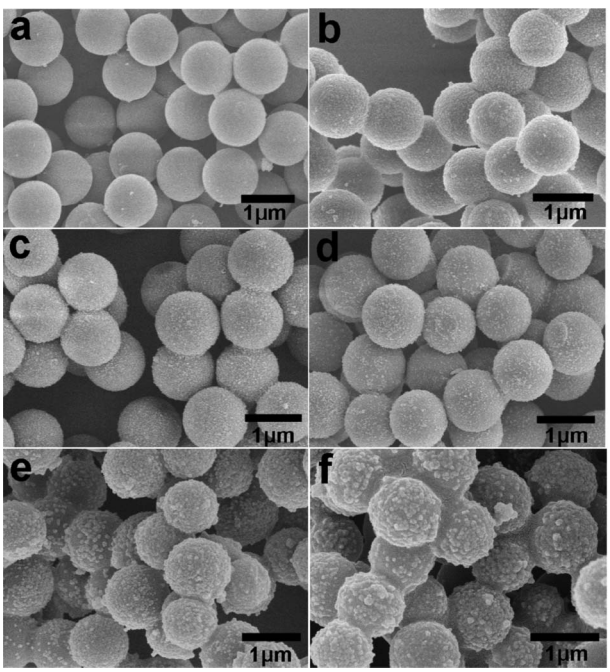

Fig. 2 Typical SEM images of as-prepared: (a) carbon spheres (b) C/CdS hybrid microspheres obtained microwave-assisted method, and after calcination at different temperatures in a N_2 flow, (c) 500, (d)600, (e)700 and (f) 800 °C.

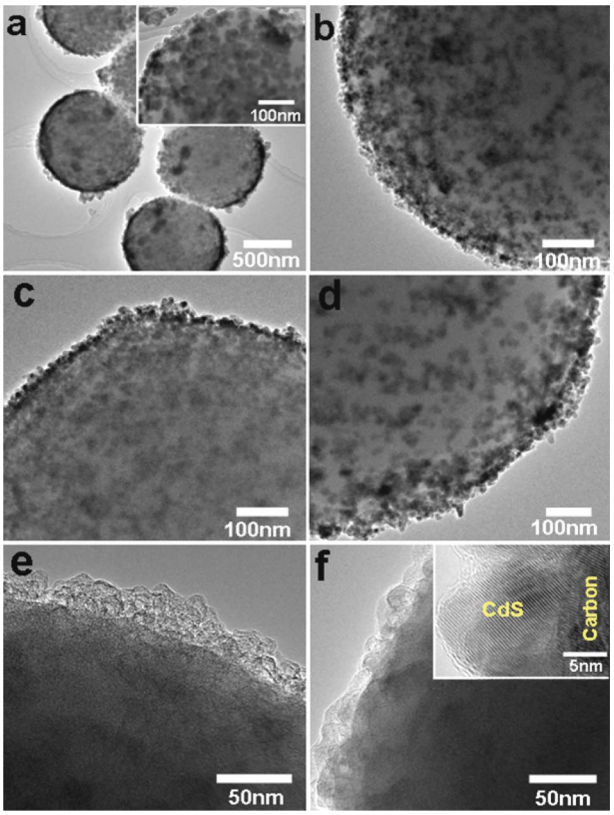

Fig. 3 Typical TEM images of as-prepared: (a) C/CdS hybrid microspheres obtained *via* microwave irradiation, and higher magnification image (inset), and after calcination at different temperatures in a N_2 flow (b) 300, (c) 400, (d)500, (e)700, (f) 800 °C and HRTEM image (inset).

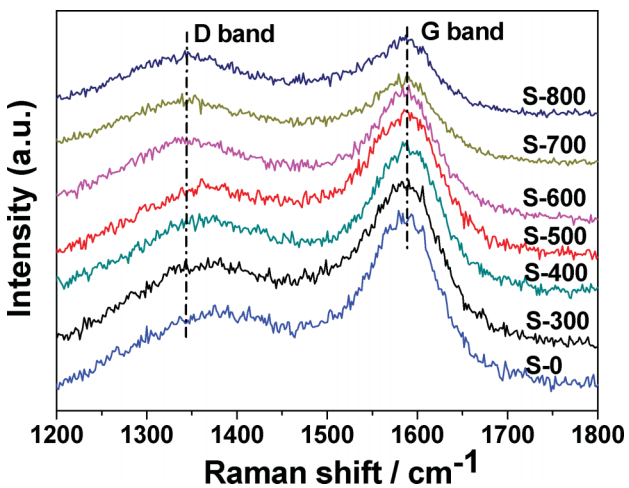

Fig. 4 Raman spectra of as-prepared C/CdS hybrid microspheres and samples after calcination at different temperatures in a N_2 flow for 3 h.

suggests that graphitization reaction below 600 °C is not high enough to form a high ordered graphite structure. When the temperature rises to 600 °C, the ratio is 0.926, the intensity of the G-band, associated with ordered graphitic-like carbon, is almost equivalent to that of the D-band. The ratio increases as the temperature is increased, which indicates that samples at a higher temperature form a more ordered carbon structure during the graphitization process.

Fig. 5 shows the FT-IR spectral analysis of the as-prepared C/CdS hybrid microspheres and samples obtained after calcination at different temperatures. Compared with the standard spectrum, the following absorption bands can be observed. The spectra of the samples show an absorption peak at 3441 cm^{-1}, which corresponds to the stretching vibration of –OH groups. The bands at 1700 $cm^{-1}$are attributed to C=O vibrations. The bands reveal that there are large numbers of hydrated residues such as –OH and COO^- groups on the surface before calcining.[22] However, after annealing treatment in a N_2 flow, the peaks corresponding to the modes of COO^- are no longer present, and the intensity of the absorption peak at 3441 cm^{-1} relating to surface –OH is significantly decreased, which may be ascribed to the thermal decarboxylation and dehydration during the higher temperature calcination process.[25] The disappearance of the C=O vibration band indicates the formation of graphitic structures, which increases the number of aromatic domains of smaller average size in graphitic structures and leads to an increase of the I_D/I_G ratio.[26,27] The reduced surface oxygen-containing functional groups (–OH and C=O) also indicates more complete graphitization, which is in good agreement with the results of the Raman spectroscopy.

To investigate the optical properties of the samples and their potential application as photonic materials, their PL spectra were recorded at room temperature. Fig. 6 shows the PL spectra of the as-prepared samples with different annealing temperatures. As expected, the as-prepared C/CdS hybrid structures all feature a broad green emission at around 491 nm under an excitation wavelength of 337 nm. There is no obvious variation in the analysis of PL spectra of the band gap energy of CdS when the composites were annealed at different temperatures. The emission peak at around 491 nm may be assigned to the radiative recombination of charge carriers immobilized in deep-trap states of different energies.[28] In addition, Sivasubramanian *et al.* have also reported that in the CdS cubic phase the position of the PL peak remains nearly unchanged when annealed in argon atmosphere.[29] The PL peak intensity of the C/CdS hybrid microspheres gradually decreased with increasing annealing temperatures, and the intensity for the S-800 is much weaker

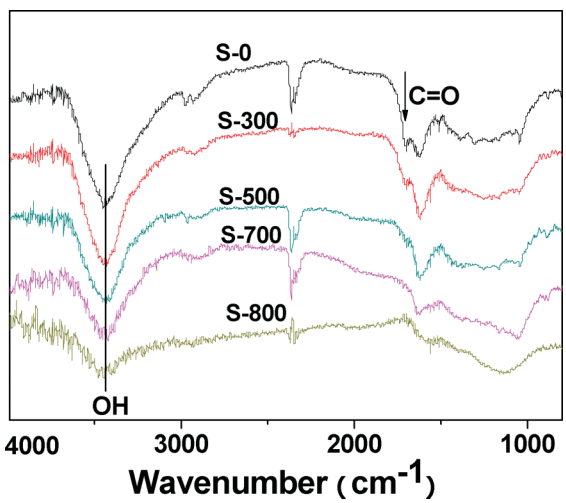

Fig. 5 FT-IR spectra of as-prepared C/CdS hybrid microspheres and samples after calcination at different temperatures in a N_2 flow for 3 h.

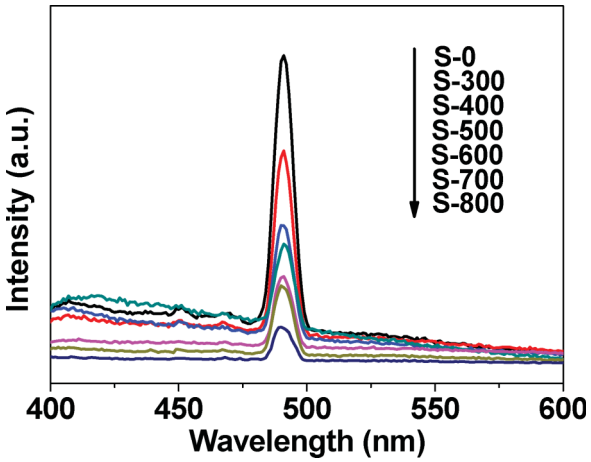

Fig. 6 PL spectra of the as-prepared C/CdS hybrid microspheres and samples after calcination at different temperatures in a N_2 flow for 3 h (λ_{ex} = 337 nm).

than that for the other samples. The differences in the PL intensities may occur due to the interface between the CdS and graphite-like carbon and the enhanced separation efficiency of the electron–hole pairs,[30] and this result is also in accord with that of Raman.

To further investigate the relationship of the sample's surface structures and the photocatalytic efficiency, the change in the concentration of RhB (C/C_0) with different exposure times under visible-light irradiation in the presence of the as-prepared samples and blank are shown in Fig. 7a, where C is the concentration of RhB at the irradiation time T and C_0 is the concentration in the absorption equilibrium of the photocatalysts before irradiation. The degradation rate of RhB by different samples after exposure to visible-light irradiation for 30 min is plotted in Fig. 7b. From these patterns, the photocatalytic activity of the samples is increasing gradually as the calcination temperature increases, which is in agreement with the result of PL. But compared to sample S-0, samples S-300, S-400, S-500 show lower photocatalytic activity. We think the photocatalytic efficiency of the C/CdS hybrid catalyst is mainly governed by surface area, crystallinity, and adsorption ability. The interface changes between the CdS nanoparticles and carbon layer will result in different factors possessing predominance. The surface of the carbon microspheres is hydrophilic and has a distribution of –OH and C=O groups before calcination, which can act as a good adsorbent for RhB, and the increasing concentration of RhB around the sample S-0 leads to the superior photocatalytic activity.[21,31] To further explain this issue, the adsorbability of RhB using different carbon microspheres obtained at different calcination temperatures as adsorbent was tested and is shown in Fig. S2.† It can be seen that about 36.1, 6.7, 7, 5.7, 2.6, 0.9 and 0.3% of RhB solution was adsorbed by carbon microspheres calcined at 0, 300, 400, 500, 600, 700, 800 °C, respectively. We now attribute this to the changing hydrophilicity of the carbon surface: the surface of carbon spheres is hydrophilic and has a distribution of –OH and C=O groups before calcination. However, after heat treatment in a N_2 flow, these groups will be significantly decreased, due to the thermal decarboxylation and dehydration during the higher temperature calcination process.[24] Thus, the adsorption capacity of the carbon will rapidly weaken after calcination.

Therefore, the superior photocatalytic performance of S-600, S-700 and S-800 can be ascribed to the ordered carbon structure during the graphitization process. The interface between graphite-like carbon and CdS is considered to be an important factor affecting the photocatalytic activity of hybrids at high-temperature calcination. Graphite-like carbon has a conjugated structure, which could be used as an electron transfer channel for reducing the recombination of the photogenerated electron–holes, and leading to improved photoconversion efficiency of the photocatalytic materials.[18] Fig. S3† illustrates the principle of charge separation in C/CdS core–shell hybrid microspheres. Raman spectroscopy also indicates that the samples at higher temperature form a more ordered carbon structure during the graphitization process. Thus, the better crystallinity and graphite-like carbon layer will give priority to the enhanced photocatalytic activity in the high temperature calcination process, which results in sample S-800 possess the best photocatalytic efficiency.

Conclusions

In summary, a series of C/CdS core–shell hybrid microspheres were obtained by calcining at different temperatures in a N_2 atmosphere. The changes of interface to influence to photochemical activities toward degradation of RhB were studied thoroughly. The results show the absorption ability for the

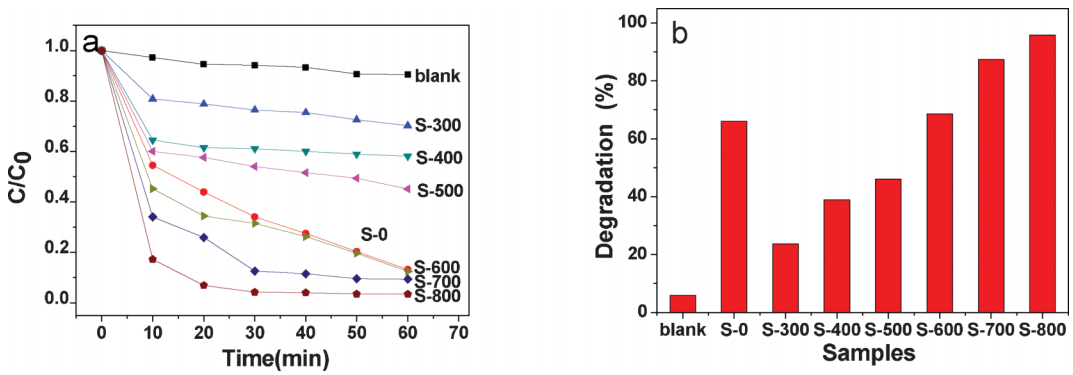

Fig. 7 (a) The relationship of the degradation efficiency of RhB in the presence of different samples and blank under visible-light irradiation, (b) the degradation rate of RhB using different samples as photocatalyst after exposure to visible-light irradiation for 30 min.

organic pollute is predominate factor in the low temperature calcination process. But for the higher temperature calcination, the better crystallinity and graphite-like carbon layer will give priority to the enhanced photocatalytic activity. These results demonstrate that *in situ* graphitization is significant in improving the photocatalytic efficiency of C/CdS hybrid microspheres. Thus, we think this new paradigm for designing more active photocatalysts will have a wide range of applications.

Acknowledgements

Financial support from the Natural Science Foundation of China (21171146), Zhejiang Provincial Natural Science Foundation of China (Y4110304) and Zhejiang Qianjiang Talent Project (2010R10025) is gratefully acknowledged. J. F. Chen acknowledges the financial support from the Anhui Provincial Natural Science Foundation (11040606M53).

References

1 C. Galindo, P. Jacques and A. Kalt, *J. Photochem. Photobiol., A*, 2001, **141**, 47.
2 M. R. Hoffmann, S. T. Martin, W. Y. Choi and D. W. Bahnemann, *Chem. Rev.*, 1995, **95**, 69.
3 Y. Hu, H. H. Qian, Y. Liu, G. H. Du, F. M. Zhang, L. B. Wang and X. Hu, *CrystEngComm*, 2011, **13**, 3438.
4 J. Cao, J. Z. Sun, J. Hong, H. Y. Li, H. Z. Chen and M. Wang, *Adv. Mater.*, 2004, **16**, 84.
5 Y. Liu, L. Zhou, Y. Hu, C. F. Guo, H. S. Qian and X. W. Lou, *J. Mater. Chem.*, 2011, **21**, 18359.
6 S. Karan and B. Mallik, *J. Phys. Chem. C*, 2007, **111**, 16734.
7 A. Podborska, B. Gaweł, Ł. Pietrzak, I. B. Szymańska, J. K. Jeszka, W. Łasocha and K. Szaciłowski, *J. Phys. Chem. C*, 2009, **113**, 6774.
8 L. M. Shen, N. Z. Bao, P. E. Prevelige and A. Gupta, *J. Phys. Chem. C*, 2010, **114**, 2551.
9 X. L. Wang, Z. C. Feng, J. Y. Shi, G. Q. Jia, S. Shen, J. Zhou and C. Li, *Phys. Chem. Chem. Phys.*, 2010, **12**, 7083.
10 J. Ma, G. A. Tai and W. L. Guo, *Ultrason. Sonochem.*, 2010, **17**, 534.
11 B. Pal, T. Torimoto, K. Iwasaki, T. Shibayama, H. Takahashi and B. Ohtani, *J. Appl. Electrochem.*, 2005, **35**, 751.
12 G. S. Li, D. Q. Zhang and J. C. Yu, *Environ. Sci. Technol.*, 2009, **43**, 7079.
13 H. B. Lu, H. Li, L. Liao, J. C. Li, Y. Tian, M. Shuai, M. F. Hu and B. P. Zhu, *Nanotechnology*, 2008, **19**, 045605.
14 Y. Liu, L. Yu, Y. Hu, C. F. Guo, F. M. Zhang and X. W. Lou, *Nanoscale*, 2012, **4**, 183.
15 G. Yu, J. Gao, J. C. Hummelen, F. Wudl and A. J. Heeger, *Science*, 1995, **270**, 1789.
16 W. L. Ma, C. Y. Yang, X. Gong, K. Lee and A. J. Heeger, *Adv. Funct. Mater.*, 2005, **15**, 1617.
17 J. Zhong, F. Chen and J. L. Zhang, *J. Phys. Chem. C*, 2010, **114**, 933.
18 L. W. Zhang, H. B. Fu and Y. F. Zhu, *Adv. Funct. Mater.*, 2008, **18**, 2180.
19 L. W. Zhang, H. Y. Cheng, R. L. Zong and Y. F. Zhu, *J. Phys. Chem. C*, 2009, **113**, 2368.
20 Y. Y. Li, J. P. Liu, X. T. Huang and J. G. Yu, *Dalton Trans.*, 2010, **39**, 3420.
21 Y. Hu, Y. Liu, H. S. Qian, Z. Q. Li and J. F. Chen, *Langmuir*, 2010, **26**, 18570.
22 X. M. Sun and Y. D. Li, *Angew. Chem., Int. Ed.*, 2004, **43**, 597.
23 W. J. Gao, Y. Wan, Y. Q. Dou and D. Y. Zhao, *Adv. Energy Mater.*, 2011, **1**, 115.
24 S. Shanmugam, A. Gabashvili, D. S. Jacob, J. C. Yu and A. Gedanken, *Chem. Mater.*, 2006, **18**, 2275.
25 S. Shlomo and N. Yaacov, *J. Therm. Anal. Calorim.*, 2011, **105**, 883.
26 S. Stankovich, D. A. Dikin, R. D. Piner, K. A. Kohlhaas, A. Kleinhammes, Y. Jia, Y. Wu, S. T. Nguyen and R. S. Ruoff, *Carbon*, 2007, **45**, 1558.
27 W. F. Chen, L. F. Yan and P. R. Bangal, *J. Phys. Chem. C*, 2010, **114**, 19885.
28 L. Spanhel, M. Haase, H. Weller and A. Henglein, *J. Am. Chem. Soc.*, 1987, **109**, 5649.
29 V. Sivasubramanian, A. K. Arora, M. Premila, C. S. Sundar and V. S. Sastry, *Phys. E.*, 2006, **31**, 93.
30 J. G. Yu, T. T. Ma and S. W. Liu, *Phys. Chem. Chem. Phys.*, 2011, **13**, 3491.
31 Y. Guo, H. S. Wang, C. L. He, L. J. Qiu and X. B. Cao, *Langmuir*, 2009, **25**, 4678.

